CHALMERS
UNIVERSITY OF TECHNOLOGY

Electrolyte recovery from spent Lithium-Ion batteries using a low temperature thermal treatment process

Downloaded from: https://research.chalmers.se, 2025-12-04 17:52 UTC

Citation for the original published paper (version of record):
Zachmann, N., Petranikova, M., Ebin, B. (2023). Electrolyte recovery from spent Lithium-Ion batteries using a low temperature thermal treatment
process. Journal of Industrial and Engineering Chemistry, 118: 351-361.
http://dx.doi.org/10.1016/j.jiec.2022.11.020

N.B. When citing this work, cite the original published paper.

research.chalmers.se offers the possibility of retrieving research publications produced at Chalmers University of Technology. It covers all kind of research output: articles, dissertations, conference papers, reports etc. since 2004. research.chalmers.se is administrated and maintained by Chalmers Library

(article starts on next page)

Journal of Industrial and Engineering Chemistry 118 (2023) 351–361

Contents lists available at ScienceDirect

Journal of Industrial and Engineering Chemistry

journal homepage: www.elsevier.com/locate/jiec

Electrolyte recovery from spent Lithium-Ion batteries using a low temperature thermal treatment process

Nils Zachmann *, Martina Petranikova, Burçak Ebin

Chalmers University of Technology, Department of Chemistry and Chemical Engineering, Nuclear Chemistry and Industrial Material Recycling, S-412 96 Gothenburg, Sweden

ARTICLE INFO

Article history:
Received 11 July 2022
Revised 13 October 2022
Accepted 10 November 2022
Available online 15 November 2022

Keywords:
Lithium-Ion batteries
Recycling process
Electrolyte
Thermal treatment
Spectroscopy analysis
Exhaust gas characterization

ABSTRACT

Electrolyte recovery is seldomly considered in state-of-art lithium-ion battery recycling methods but rather evaporates and decomposes uncontrolled during the pre-treatment steps. However, controlled and safe removal of the electrolyte is inevitable and of high importance to the recycling industry to minimize the environmental impact of the recycling processes by preventing severe threats produced by the inflammable, toxic and hazardous components of the electrolyte. This study investigated the effects of temperature and process time of a low temperature thermal treatment process on electrolyte recovery. The process exhaust gases and recovered products were analyzed by In-Situ Fourier-transform infrared spectroscopy (FT-IR) and gas chromatography-mass spectrometry (GC–MS) to determine the effectiveness of the significant process parameters. The results show that the electrolyte solvents, which are dimethyl carbonate (DMC), ethyl methyl carbonate (EMC), and ethylene carbonate (EC), were successfully recovered for 80 minutes of processing time at 130 °C. The $LiPF_6$ decomposition products hydrogen fluoride (HF) and phosphoryl fluoride (POF_3) were detected in the exhaust gas stream and recovered as acidic solutions. Thermal treatment below 150 °C is a promising approach for the recovery of the electrolyte solvents prior to the metal recycling stage due to its simplicity, feasibility, and environmental benefit.

© 2022 The Authors. Published by Elsevier B.V. on behalf of The Korean Society of Industrial and Engineering Chemistry. This is an open access article under the CC BY license (http://creativecommons.org/licenses/by/4.0/).

Introduction

The first commercialized rechargeable Lithium Ion-battery (LiB) was released by Sony and Asahi Kasei in 1991. Over the last few years, different types of LiBs (NMC, LCO, LMO, NCA, LFP) have been developed and refined to improve their already preferable combination of high energy and power density as well as their relatively long service-life [1,2]. Whereas the exact material composition and format of the battery cell differs within the different types of LiBs and their specific application, the standard battery cell is generally composed of a layered structure of anode (15–25 wt%), separator (4–10 wt%) and cathode (25–35 wt%) embedded by the electrolyte (10–20 wt%) [3]. Although the weight is almost evenly distributed among the four components, the value contribution of the battery cell is mainly concentrated in the active materials on the cathode side. Hence, driven by the economic interest, the recycling of LiBs is mainly orientated on the most valuable components cobalt (Co), nickel (Ni), copper (Cu), and lithium (Li). A new proposal by the European Commission, created to modernize and replace the EU's battery directive from 2006 [4–6], integrated measures on the end-of-life management of LiBs. In particular, a minimum recycling content and recycling efficiency to tackle the environmental and social impacts in all stages of the LiB life cycle was announced [6]. Thereby, an overall lithium-ion battery recycling efficiency by weight percent was declared and appointed to reach at least 65 wt % by 2025 and 70 wt% by 2030 [5,6]. However, by neglecting the recovery of the less valuable components, such as the electrolyte and the separator, it will be challenging to reach the desired overall LiB recycling efficiency targets in the proposed EU battery directive.

Due to the complexity of the battery assembly and the raw materials, a combination of physical pre-treatment, thermal treatment, and hydrometallurgy processes is required for the recycling purpose. Manual, mechanical and/or thermal pre-treatment is necessary to reclaim the electrode materials prior to the hydrometallurgy steps such as leaching, solvent extraction, and filtration process in which the transition metals (Li, Co, Ni) are conventionally recovered [7,8]. The pre-treatment methods consist mainly of discharging, dismantling, crushing followed by magnetic/mechanical separation and screening. Thermal treatment (pyrolysis or incineration) at 550 °C is used to liberate the active materials by

* Corresponding author.
E-mail address: zachmann@chalmers.se (N. Zachmann).

https://doi.org/10.1016/j.jiec.2022.11.020
1226-086X/© 2022 The Authors. Published by Elsevier B.V. on behalf of The Korean Society of Industrial and Engineering Chemistry.
This is an open access article under the CC BY license (http://creativecommons.org/licenses/by/4.0/).

decomposition of the binder material, polyvinylidene fluoride (PVDF). During the thermal treatment steps, most organics (binder material and separator) decompose and can hardly be reutilized [8,9]. Moreover, during the mechanical pre-treatment process, the electrolyte may evaporate uncontrolled and eventually degrade at the elevated thermal treatment temperatures, which leads to undesired losses of potentially recoverable material [10,11].

The liquid electrolyte in LiBs is a multicomponent system composed of a conductive salt, mostly $LiPF_6$, dissolved in a mixture of (volatile) linear and cyclic carbonates and potential additives. Commonly the electrolyte solvent mixture consists of dimethyl carbonate (DMC), ethyl methyl carbonate (EMC), dimethyl carbonate (DEC), propylene carbonate (PC) and/or ethylene carbonate (EC) [12].

In another perspective, electrolyte extraction is important in respect to environmental pollution and safety aspects. Severe threats can be potentially induced by the inflammable, toxic, and hazardous components of the organic solvents and the fluorinated decomposition products of the conductive salt [10,11,13,14]. Therefore, uncontrolled evaporation of the electrolyte leads not only to an enormous risk regarding working safety in recycling plants and the environment but also to a potential serious disturbance or even damage of the recycling process plant [15]. Furthermore, mechanical processing generates secondary waste (e.g. separator) which is potentially contaminated with the electrolyte solvents and therefore requires special expensive disposal [16]. Consequently, controlled and safe removal of the electrolyte before the common mechanical processing and thermal treatment methods prior to the metal recycling stage is inevitable to minimize the environmental impact of the recycling process.

Recently, electrolyte recovery has been attracting scientific and industrial attention and a few approaches have been investigated, such as supercritical fluid extraction, solvent extraction, and vacuum distillation. Grützke et al. [17] developed a supercritical helium head pressure carbon dioxide ($scHHPCO_2$) procedure to extract the organic solvents DMC, EMC, EC, traces of the conductive salt $LiPF_6$ and electrolyte aging products from a jelly roll of commercial 18,850 cells. The recovery rates and extract composition in the process strongly depended on the extracted material and the process recovery rate of the electrolyte solvent was low at a considerable long extraction time. In a subsequent study, Grützke et al. [18] achieved an extraction yield of 89.1 ± 3.4% of the electrolyte mixture (DMC, EMC, EC, $LiPF_6$) from the jelly roll of commercial 18,650 LiB cells using a flow-through liquid CO_2 (25 °C, 60 bar, 15 L/min) extraction procedure and acetonnitrile/PC as a co-solvent. However, the recovery efficiency and extract composition in the process were sensitive and strongly dependent on the extraction conditions (pressure, temperature and time). Especially, EC and $LiPF_6$ demand an additional co-solvent to achieve reasonable extraction yields. Mu et al. [19] claim a high separation of an electrolyte mixture of EC, PC, DMC, EMC and $LiPF_6$ from a polypropylene separator using a combination of static and dynamic transcritical CO_2 (28.86 °C, 8.84 Mpa, 9.77 min) extraction method.

Other approaches to recycle the electrolyte are solvent extraction or thermal treatment methods. He et al. [20] claimed an electrolyte separation yield of 95.6% (PC, EC, $LiPF_6$) from spent LiB battery cells using a house-made complex aqueous peeling agent, namely exfoliating and extracting solution (AEES). During the process, the conductive salt $LiPF_6$ was converted into $NaPF_6$ and Li salt. A drawback is a requirement of a manual stripping of the electrodes and separator before the process, which is labor and time-consuming and causes evaporation of the electrolyte. Moreover, the separation process was only validated on an electrolyte mixture consisting of PC and EC. Zhong et al. [8] claim a high electrolyte solvent separation yield of spent $LiFePO_4$ batteries without any specification of the (reclaimed) electrolyte composition using low temperature volatilization at 120 °C followed after a discharge and crushing step. After the separation of the electrolyte at low temperature, organic electrolyte products and light alkenes were found in the pyrolysis gas at elevated temperatures.

Although the studies focused on the extraction of the LiB electrolyte, there is a lack of systematic investigation of the recovered products and process exhaust gas emissions. Potential toxic exhaust gas emissions originated from decomposition products of the conductive salt can lead to enormous environmental effects and risks regarding working safety [14]. Therefore, for proper handling of the process exhaust gas a precise understanding of its composition and occurrence is of high importance.

In this study, a low temperature thermal treatment process at different temperatures (90 °C–150 °C) to recover the electrolyte of spent LiBs was studied. The composition of the recovered electrolyte was analyzed by gas chromatography-mass spectrometry (GC–MS), attenuated total reflection Fourier-transform infrared spectroscopy (ATR-FTIR) and X-Ray diffraction analysis (XRD). Furthermore, the exhaust gas emissions were analyzed by In-Situ FT-IR to determine its composition and to study its toxicity originating from the decomposition products of the conductive salt. The optimal process temperature and duration of the low temperature thermal treatment process was investigated. Electrolyte recovery by low temperature thermal treatment prior to the metal recycling stage is a promising new approach due to its simplicity, feasibility, and environmental benefits.

Experimental

Materials and reagents

Spent lithium-ion battery pouch cells (NMC/graphite) of an EV application were used in this study. Nitrogen (N_2) gas with a purity of 99.9% was used in the experiments. HNO_3 (>65%), acetone (>95%), acetonitrile (>99.9%), EMC (>99%), and EC (>99%) were purchased from Merck Millipore and dry ice from Cryotech.

Experimental procedures

Sample preparation

Discharged commercial NMC battery cells were stored for 2 days at −18 °C to minimize the evaporation of the volatile electrolyte solvents during the cell opening. The pouch of the battery cell was opened and the pouch cell electrode stack (several layers of anode, separator, and cathode) was removed manually by slicing along the edges with a sharp knife. Before each thermal treatment experiment, rectangular pieces with dimensions of 9x1cm (11.07 ± 0.95 g) were cut from the electrode stack with a scalpel. Between every experimental run, the electrode stack was stored inside a sealed plastic bag at −18 °C.

Experimental method

A flowsheet of the experimental method is given in Figure S1 in the Supportive Material. The experimental setup of the thermal treatment process is illustrated in Fig. 1. It consisted of a quartz tube placed inside a tube furnace (RT 50-250/13, Nabertherm). Nitrogen flow (340 ml/min) was controlled by a valve and measured by a flowmeter. The outlet of the quartz tube was either connected to a gas cell with flat glass CaF_2 windows and an optical path length of 10 cm or to a collection vial placed in a cold trap with a mixture of dry ice and acetone at −78 °C (see Fig. 1). Thereafter, a gas washing bottle filled with 50 ml MQ water was connected. The temperature of the furnace was set to 90°C, 110°C,

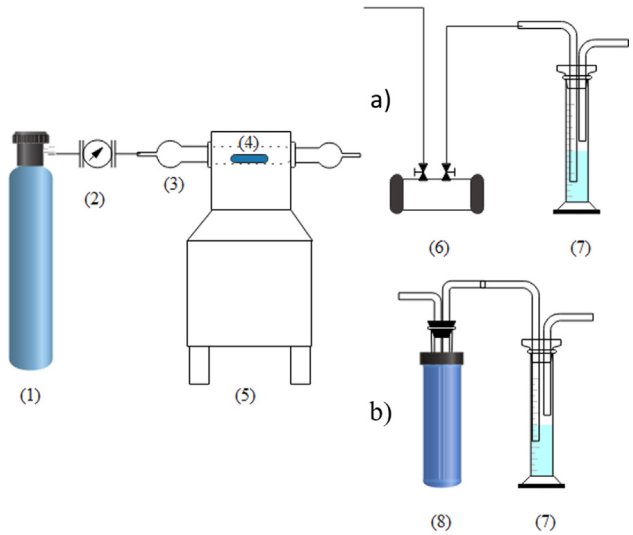

Fig. 1. Illustration of the experimental set up of the thermal treatment process for (a) In-Situ FT-IR analysis and (b) cryogenically trapping of the process exhaust gas. (1) Nitrogen gas supply, (2) Flowmeter, (3) Quartz tube, (4) Sample in ceramic combustion boat, (5) Tube furnace, (6) Gas cell, (7) Gas washing bottle, and (8) Collection vial in cold trap.

130°C, and 150°C, and monitored by a thermocouple connected to a data logger (TC-08, Pico Technology).

The battery sample was put into a ceramic combustion boat and first inserted to the quartz tube outside the tube furnace for 5 minutes to equilibrate the N_2 environment inside the quartz tube. Then, the ceramic combustion boat together with the sample was pushed into the middle of the furnace under N_2 atmosphere. After the thermal treatment process time of 3 hours, the combustion boat was removed from the furnace at the reaction temperature and subsequently cooled at room temperature. Before and after the thermal treatment process, the weight of the battery sample was measured with a high precision scale under air.

The thermal treatment process for each temperature setting was conducted in triplicates in random order. The exhaust gas of the thermal treatment processes of two experimental runs of each triplicate for all samples were frequently monitored by In-Situ FT-IR spectroscopy with a scan rate of 40 seconds. In the third experimental run, the exhaust gas was directly cryogenically trapped in a sample vial placed in a cold trap with a mixture of dry ice and acetone at −78 °C to collect the electrolyte. The recovered liquid was characterized by GC–MS. In all the experimental runs the exhaust gas was washed by a gas washing bottle filled with 50 ml MQ water before its release into the environment. The gas washing water was analyzed with Ion chromatography and the pH was measured.

Condensation residues on the walls of the quartz tube outside the furnace were collected after the setup cooled down and characterized by ATR FT-IR, XRD, and ICP-OES.

Measurement and characterization

Thermogravimetric analysis (TGA) was carried out using a thermogravimetric analyzer (Q500, TA Instruments) in a temperature range between 20 °C and 300 °C with a constant nitrogen gas flow of 100 ml/min. The heating rate was maximum 5 °C/min with a high-resolution sensitivity of 4.0 and a resolution of 5.0, which is a specific analysis method of the equipment. Thereby, determined by the weight change of the sample, the heating rate of the furnace was automatically reduced and controlled by the equipment to obtain better and higher resolution results. The TGA sample weight was 20.99 ± 0.01 mg.

The thermal treatment process exhaust gas was analyzed with In-Situ FT-IR. The infrared spectra were continuously recorded by an FT-IR spectrometer (Spectrum Two, Perkin Elmer) in the range of 4000 cm^{-1} to 900 cm^{-1} with a resolution of 4 cm^{-1}. The scan time per spectrum was selected to be 40 seconds corresponding to approximately 12 scans. Pure N_2 with the experimental flow rate of 340 ml/min in an empty run was used as a background. The reference spectra of EC and EMC in the gas phase were obtained by evaporation of a few droplets of liquid EMC and EC, separately, inside the gas cell while monitoring the FT-IR spectra. The In-Situ FT-IR spectra of the gas emission were analyzed to study the composition of the process exhaust gas and to determine the time evolution of the detected peaks. For the latter the strong characteristic peaks of the detected components were plotted over the experimental time of 180 minutes. The attenuated total reflection (ATR) method of the FT-IR spectrometer was used to characterize the collected crystalline condensate from the quartz tube walls after the thermal treatment process. The spectra were recorded in a range of 4000 cm^{-1} to 450 cm^{-1} with a resolution of 2 cm^{-1} and a total of 32 scans.

X-ray diffraction analysis (XRD, Bruker D8 Advance) was used to determine the crystallographic structure of the recovered condensate to determine the crystalline substance. Subsequently, the recovered condensate was dissolved in 0.5 M HNO_3 (5 ml) and filtered for elemental analysis by inductively coupled plasma optical emission spectrometry (ICP-OES, ThermoFisher Scientific, iCAP PRO).

The weight loss of the battery samples after the thermal treatment process was calculated according to Eq. (1):

$$Weight\ loss = \left(1 - \frac{m_a}{m_0}\right) \times 100 \quad (1)$$

Whereas m_0 is the initial sample weight and m_a is the sample weight after the thermal treatment process. A preliminary experiment was conducted to estimate the weight loss of the electrode stack at room temperature inside a fume hood. Therefore, the sample was prepared, placed on a scale and its weight change was frequently determined.

The recovered liquid electrolyte was analyzed by GC–MS (7890A, Agilent Technologies) with an Agilent HP-5MS 5% Phenyl Methyl Silox column (30 m × 250 µm × 0.25 µm). The samples were diluted with acetonitrile (1:150) and then injected at 250 °C with a split ratio of 1:100 and a purge flow of 3 ml/min. Helium as carrier gas with a column flow of 1 mL/min was selected. The initial column oven temperature was held for 1 min at 40 °C, then increased to 230 °C with a heat rate of 30 °C/min and held for 3 min at the final temperature. The mass spectrum in a range of 15–300 m/z was obtained in the electron ionization (EI) mode at 230 °C ion source temperature and 70 eV filament voltage.

Ion Chromatography (IC, Metrohm 771 IC Compact, DX-100, Dionex) was used to analyze the gas washing water after the thermal treatment. The samples were diluted (1:30) with MQ water and then injected (20 µl) into the column (DionexIonPac AG4A-SC, 4 × 50 mm, ThermoFisher Scientific) for anion analysis. A carbonate buffer (1.7 mM $NaHCO_3$, 1.8 mM Na_2CO_3) was used as the eluent and MQ water was used as a background sample. The presence of F^- and PO_4^{3-} were confirmed via the retention time of standard solutions.

Results and discussion

Sample characterization

Thermogravimetric analysis (TGA) of the spent LiB electrode stack was carried out to determine the organic solvent mixture in the electrolyte based on their boiling points. In addition, the

TGA result was used to set the temperature range and the furnace temperature conditions for the low temperature thermal treatment process. Fig. 2 presents the thermogravimetric (TG) and the differentiate thermogravimetric (DTG) curve of a freezer stored LiB electrode stack (20.99 ± 0.1 mg) in the temperature range of 20 °C to 300 °C. The weight loss of the electrode stack was 9.34 wt.%. Three peaks at 96 °C, 109.6 °C, and 128.9 °C were clearly observed in the DTG curve of the sample. Those temperatures are in alignment with the boiling points of DMC (90 °C), EMC (107 °C), and DEC (126 °C). However, the peak at 128.9 °C can also be associated with the onset decomposition temperature of $LiPF_6$, which is at 134.84 °C [21].

Most commonly, the electrolyte solvent mixture consists of a cyclic carbonate, such as EC or PC, mixed with linear carbonates, such as DMC, EMC, or DEC. According to the TGA results, the linear carbonates in the mixture of organic solvents of the battery cell were proposed to be a mixture of DMC, EMC, and DEC. However, no peak at temperatures corresponding to EC nor PC with boiling points at 248 °C and 242 °C, respectively, were observed. Most likely, the cyclic carbonate used in the electrolyte mixture evaporated along with the evaporated substances before their boiling point temperatures were reached. Further analysis was necessary to verify the electrolyte solvent composition of the spent LiB.

The DTG curve in Fig. 2 remains steady after 150 °C and no peaks were observed between 150 °C and 300 °C. Therefore, the maximum thermal treatment process temperature was decided as 150 °C. Based on the DTG peak positions, the other temperature settings were determined as 90 °C, 110 °C, and 130 °C.

A drop in the weight of approximately 1.4 wt% at 21.7 °C was observed in the TG curve of the electrode stack in Fig. 2. The TGA was not conducted directly after the electrode stack was removed from its storage at −18 °C. During the time the sample was transported to the instrument, the sample unfroze, and the electrolyte began to evaporate. Eventually, the volatile liquid electrolyte evaporated almost entirely. The resuming separated electrolyte during the TGA above room temperature corresponds mainly to the incorporated and immobilized electrolyte into the electrodes and the separator, and the decomposition of the conductive salt [8,15].

In addition to the TGA results, the electrolyte solvent composition of the spent battery cell sample was analyzed based on In-Situ FT-IR spectra of its exhaust at room temperature (24 °C) under constant nitrogen flow of 340 ml/min. Fig. 3 shows the FT-IR spectra of the exhaust composition of the battery sample at room temperature 1, 3, and 5 min before the combustion boat was inserted into the tube furnace. The gas phase spectra of pure DMC, EMC, and EC are plotted in Fig. 3 as the reference spectra to compare the battery exhaust spectra with the pure electrolyte solvent gas phase spectra. The reference spectrum of DMC in the gas phase was taken from the NIST database [22], whereas the gas phase reference spectra of EC and EMC were produced in-house. The obtained characteristic peaks of the spent battery cell exhaust at room temperature were compared to the reference spectra of organic solvents commonly used in electrolyte mixtures. Table 1 summarizes the vibrational peaks between 2000 cm^{-1} and 900 cm^{-1} used for the assignment of the electrolyte composition. The vibrational peaks at 1780 cm^{-1} (νC=O), 1463 cm^{-1} (CH_3 sym. def.), and 1295 cm^{-1} (ν_aO-C-O) correspond to DMC [23], whereas the peaks at 1772 cm^{-1} (νC=O), 1378 cm^{-1} (CH_3) and 1370 cm^{-1} were assigned to EMC [24]. The characteristic peaks at 1876 cm^{-1}, 1868 cm^{-1}, and 1860 cm^{-1} of the exhaust gas spectrum originate from EC [25]. Identification details are given in Table 1. However, characteristic peaks of DEC at 1766 cm^{-1} (νC=O), 1475 cm^{-1} (CH_2) and 1271 cm^{-1} (O-C-O) were not detected in the exhaust spectra [26].

Based on the exhaust gas analysis by FT-IR and the TGA results, the electrolyte solvent mixture used in the spent EV battery cell was composed of EC as the cyclic carbonate solvent as well as DMC and EMC as the linear carbonate solvents. The identification of the characteristic peaks by means of Table 1 was straightforward since no interactions between the solvents had to be considered as in the gas phase the molecules move freely.

The organic solvents of the electrolyte mixture are (highly) volatile with vapor pressures of 55.4 mmHg (DMC), 24 mmHg (EMC), and 0.045 mmHg (EC) at 25 °C in relation to the vapor pressure of water (23.8 mmHg) and the atmospheric pressure (760 mmHg) at 25 °C [14]. Instant evaporation of the electrolyte solvent mixture was monitored under low N_2 flow even at room temperature. Strong peak intensities were already monitored within the first minute. In a preliminary experiment, the weight loss of the electrode stack at room temperature (24 °C) was monitored over time. As seen in Figure S3 a weight loss of 7.4 wt% after 250 min was observed. Pronounced loss of the electrolyte during conventual pre-treatment steps such as crushing, and magnetic/mechanical separation is eventually unavoidable, considering the exhaust gas is not captured by a specific system. Consequently, recovery of the electrolyte should be performed directly after

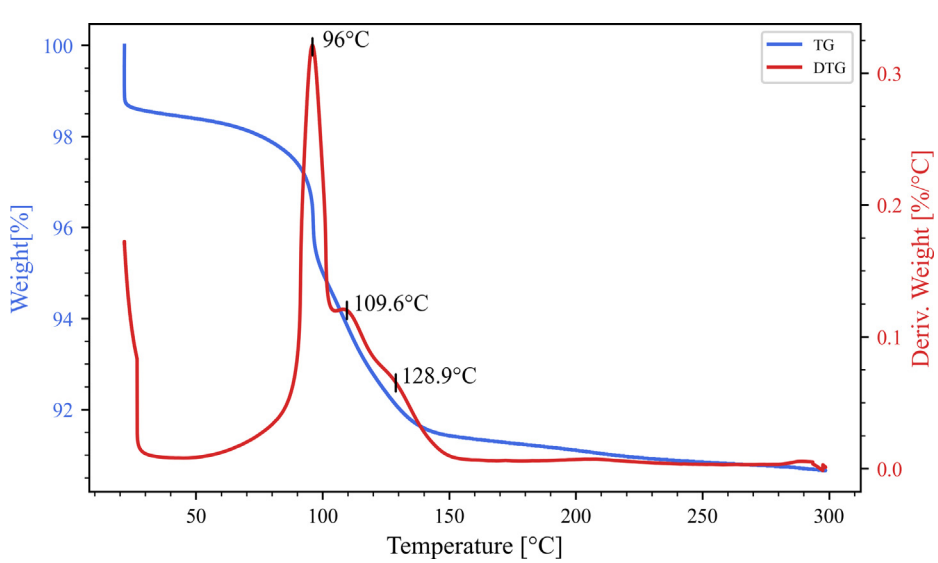

Fig. 2. TG (blue) and DTG (red) curve of the electrode stack of a freezer stored LiB cell.

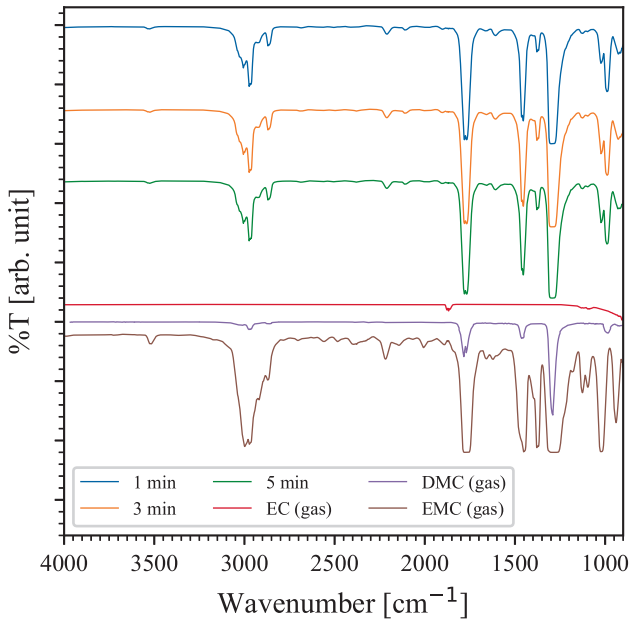

Fig. 3. FT-IR spectra of the exhaust gas composition of the battery sample at room temperature before the combustion boat was inserted into the tube furnace. 1, 3, and 5 min before the thermal treatment process. FT-IR spectra of DMC, EMC, and EC in gas phase are plotted as a reference.

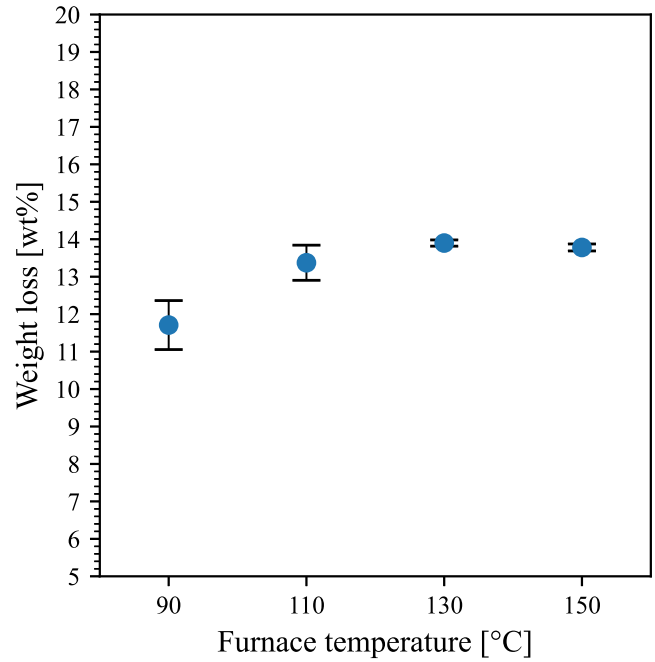

Fig. 4. Weight loss in weight percentage [wt%] after low temperature thermal treatment for 3 hours under constant nitrogen flow at different temperature conditions (90 °C, 110 °C, 130 °C and 150 °C).

opening the battery cell to maximize the electrolyte recovery yield while minimizing the environmental side effects and risks regarding working safety.

Low temperature thermal treatment

Weight loss

The weight losses in weight percent [wt%] of the spent LiB electrode stack after 3 hours at thermal treatment process temperatures at 90 °C, 110 °C, 130 °C, and 150 °C are plotted in Fig. 4. At a process temperature of 130 °C, the weight loss converged to 13.9 wt%. A noticeable point is that the standard deviation of the weight loss decreased with increasing temperature. The decreasing standard deviation may be related to the degradation of the conductive salt. It is assumed that the amount of decomposed conductive salt increases with elevated temperature. Sloop et al. [27] studied the decomposition of $LiPF_6$ and observed a weight percentage loss to 17 wt% at temperatures up to 150 °C, which corresponds to the decomposition to LiF. Accordingly, $LiPF_6$ can fully degrade at 150 °C under specific conditions. At lower temperatures, however, the degradation can be incomplete, leading to a deviation in weight loss for every experimental run.

A difference in weight loss of 4.46 wt% was observed between the TGA and the thermal treatment process, which were 9.34 wt % and 13.90 wt% at 130 °C, respectively. It was assumed that the undesired evaporation of the electrolyte solvents at room temperature prior to the thermal treatment process was minimized by storage of the sample at −18 °C. In the thermal treatment process, the initial sample weight (11.07 ± 0.95 g) was measured immediately after the sample was prepared from the freezer-stored electrode stack. It is important to state that the sample size was smaller (20.99 ± 0.1 mg) and the sample preparation and running of the equipment took a longer initiation time for TGA than the thermal treatment in the furnace. Parts of the volatile liquid electrolyte started evaporating at room temperature before the beginning of the TGA. In the low temperature thermal treatment process, the liquid electrolyte and the incorporated and immobilized electrolyte contributed to the determined mass loss.

Table 1
Summary of the characteristic peaks used for the assignments the exhaust gas FT-IR spectrum between 2000 cm^{-1} and 900 cm^{-1}. ν, δ, a and s represent stretching, bending, asymmetric and symmetric deformation.

EC [25]		DMC [23]		EMC [24]	
1876 cm^{-1}		1780 cm^{-1}	*νC=O*	1772 cm^{-1}	*νC=O*
1868 cm^{-1}	*νC=O*	1768 cm^{-1}		1764 cm^{-1}	
1860 cm^{-1}					
1385 cm^{-1}	*CH_2*	1463 cm^{-1}	*CH_3*	1452 cm^{-1}	*CH_3 sym. def (ethyl group) + CH_2 wagging*
		1454 cm^{-1}	*sym. def.*		
1131 cm^{-1}		1295 cm^{-1}	*ν_aO-C-O*	1378 cm^{-1}	*CH_3*
1122 cm^{-1}	*νRing*			1370 cm^{-1}	
1096 cm^{-1}		996 cm^{-1}		1284 cm^{-1}	*O-C-O*
1087 cm^{-1}	*νRing*	990 cm^{-1}	*νCH_3-O*		
1079 cm^{-1}		985 cm^{-1}			
		925 cm^{-1}	*νCH_3-O*	1128 cm^{-1}	*δO-C–C + CH_3 assym. def (ethyl group)*
		917 cm^{-1}			
				1096 cm^{-1}	*νCH_3-O*
				1025 cm^{-1}	*νO-C–C + νCH_3-O*
				940 cm^{-1}	*νCH_3-O-C + δC=O-C + νO-C–C*

Characterization of the collected products

In the suggested process two products were collected after the low temperature treatment. A clear liquid was obtained by trapping the exhaust gas cryogenically and a solid residue was collected from the quartz tube walls. The analysis of the collected products is discussed in the following two sections.

Liquid phase product – Cryogenically trapped exhaust gas

The process exhaust gas was cryogenically trapped over the entire thermal treatment duration in a sample vial placed in a cold trap with a mixture of dry ice and acetone at −78 °C to recover the separated electrolyte. A clear liquid was obtained and subsequently analyzed with GC–MS. The obtained chromatographs are plotted in Fig. 5. The peaks with retention times at 2.33 min, 2.81 min, and 4.59 min were clearly identified as DMC, EMC, and minor amount of EC according to the NIST 08 library.

Solid phase product – Condensate in the quartz tube

Parts of the exhaust gas condensed on the walls of the quartz tube just outside of the furnace during the thermal treatment process as seen in Fig. 6. When the set-up was cooled down to room temperature, the condensate immediately crystallized as a solid. After the thermal treatment process, roughly 0.3 g (≈ 20–25% of weight loss) of the condensate residue was collected and analyzed by FT-IR, XRD and ICP-OES to determine its composition.

FT-IR spectra of the crystalline solid residue collected after the thermal treatment at 110 °C, 130 °C and 150 °C were obtained to analyze its composition by ATR method. Fig. 7 shows the recorded FT-IR spectra compared with the spectrum of EC in solid phase served as a reference. The reference spectra of the recovered material in all conditions perfectly match with the reference spectrum of EC. Therefore, ethylene carbonate was determined as the main product of the crystalline condensate. The melting and boiling points of ethylene carbonate are 34 °C and 243 °C, respectively. The temperature of the wall of the quartz tube located outside the tube furnace was much colder than the boiling point of EC. Hence, gaseous EC condensates on the wall of the quartz tube. When the quartz tube is removed from the tube furnace, the temperature of the quartz tube wall dropped below 34 °C which led to the formation of solid EC.

The recovered material is not entirely composed of pure EC. In addition to the characteristic peaks of EC, miner peaks between 1050 cm^{-1} and 450 cm^{-1} were observed as shown in Fig. 7 b).

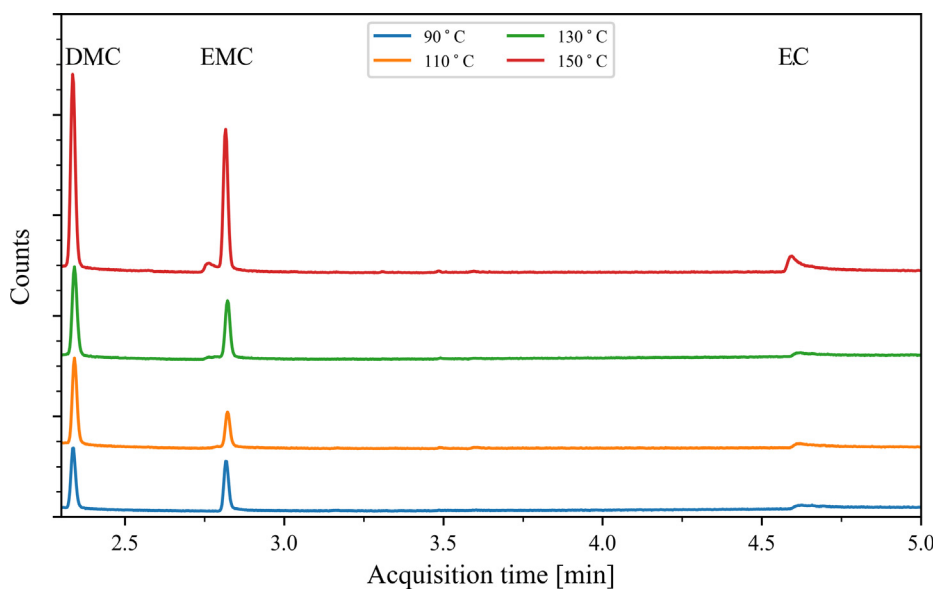

Fig. 5. Chromatograms (GC–MS) of the recovered electrolyte at different thermal treatment process temperatures of 90 °C, 110 °C, 130 °C, 150 °C.

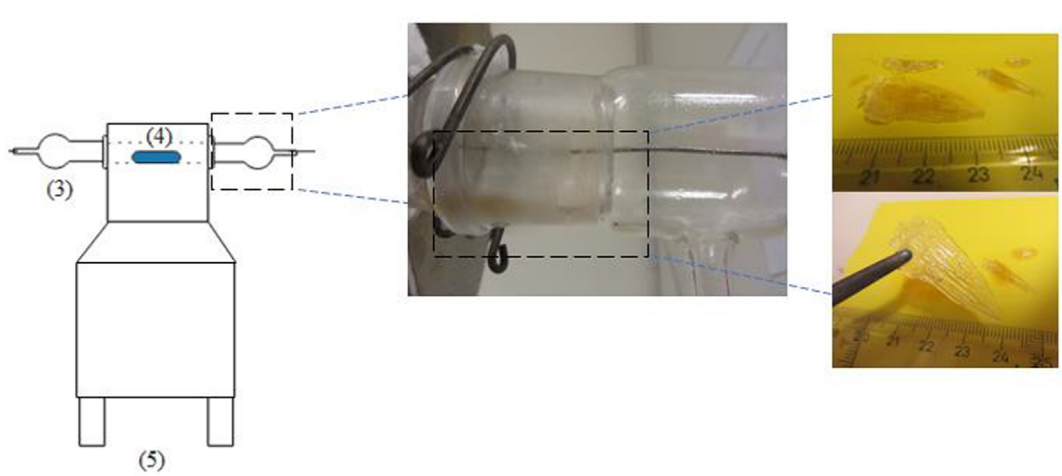

Fig. 6. Location and photograph of the condensate residue collected after the low temperature thermal treatment process.

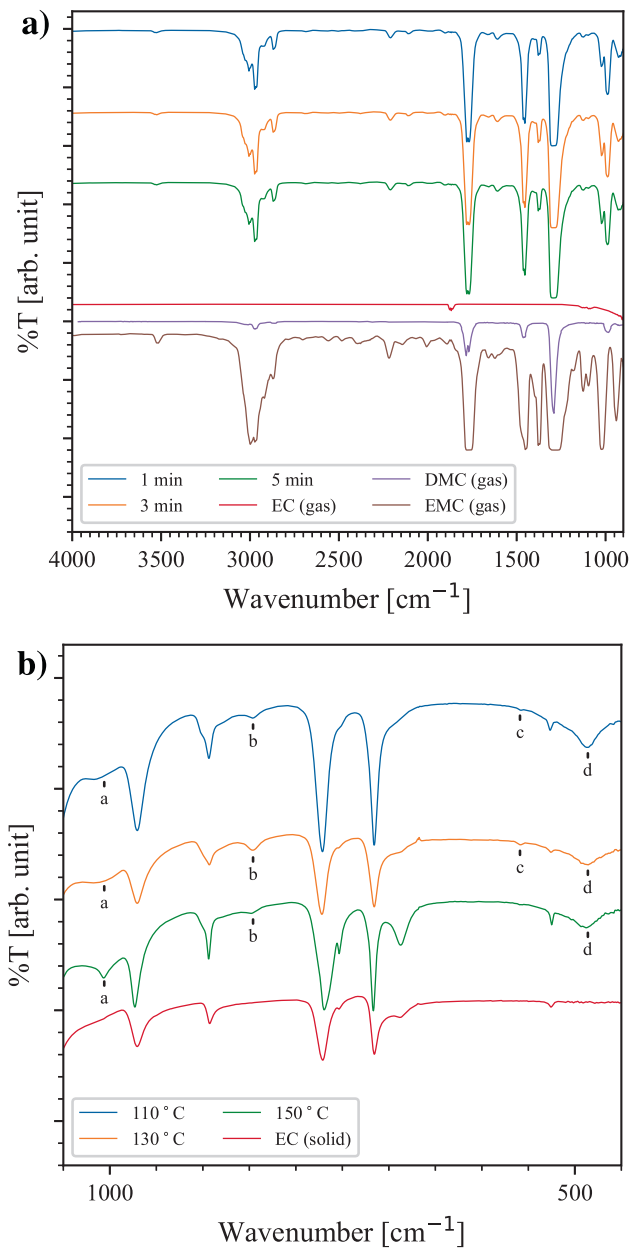

Fig. 7. FTIR spectrum of the quartz tube residue from the thermal treatment experiments at 110 °C, 130 °C, 150 °C and as a reference spectrum EC in solid phase between (a) 4000–900 cm^{-1} and (b) 1050–450 cm^{-1}. The corresponding assignments for the annotations are presented in Table 2.

These peaks were assigned as given in Table 2 to the vibrational modes of POF_3 (a, d) and $LiPF_6$ (b, c), the conductive salt.

XRD analysis was conducted to analyze the crystallographic structure of the recovered condensate from the quartz tube walls. The diffraction pattern of the recovered condensate after thermal treatment at 130 °C and 150 °C in the range from 10° to 55° 2Θ is plotted in Fig. 8. The diffraction peaks correspond to the characteristic peaks of EC with a monoclinic crystal structure (PDF Card No: 00-008-0768).

Subsequent to the XRD analysis, the condensate was dissolved in 0.5 M HNO_3 (5 ml) for analysis by ICP-OES. Thereby, traces of Li (0.8 ppm), Mn (2.3 ppm), Co (0.94 ppm), Cu (1.29 ppm), Ni (0.57 ppm), and Al (0.16 ppm) were observed.

Table 2
Wavenumber and corresponding assignment for the annotations given in Fig. 7.

Annotation	Wavenumber [cm^{-1}]	Assignment
a	1014	POF_3 (P=O)
b	846	$LiPF_6$ (P-F)
c	559	$LiPF_6$ (F-P-F)
d	487	POF_3 (O=PF_3)

Exhaust gas analysis by In-Situ FT-IR

The exhaust gas of the low temperature thermal treatment process was analyzed with In-Situ FT-IR, where the exhaust gas was continuously monitored over the entire experimental period with a scan rate of 40 seconds per spectrum for all experimental sets. The FT-IR spectra of the thermal treatment process exhaust gas after 1 min, 15 min, 30 min, 60 min, 90 min, 120 min, and 180 min at 90 °C, 110 °C, 130 °C, and 150 °C are plotted in Fig. 9. Strong characteristic peak intensities of DMC and EMC – up to 100%T – were directly detected at the first minute of the process (see Table 1). The peak intensities decreased over the process time of 180 minutes.

The optimum process duration was determined based on the In-Situ FT-IR spectra of the thermal treatment exhaust gas. Fig. 10 shows the relative absorption intensity of selected characteristic peaks of DMC and EMC over the entire process time of 180 minutes, whereas the equilibration time is denoted as −5 to 0 min before feeding the sample. The characteristic peaks at 1780 cm^{-1} belonging to νC=O of DMC and at 1284 cm^{-1} corresponding to νO-C-O vibration of EMC were selected based on their strong peak intensities and selectivity. Evaporation of DMC and EMC was observed before the sample was exposed to the process temperature. Relative absorption intensities above 74% (C=O peak, DMC) and 90% (O-C-O peak, EMC) were observed between −5 and 0 min. Regardless of the process temperature, the relative absorption intensity increased to 100% after the sample was pushed into the furnace. After 40 minutes the intensity started to vanish and finally levels off at 60 minutes for νC=O peak and 80 minutes for νO-C-O peak. Consequently, the optimum low temperature thermal treatment process time for the recovery of the electrolyte solvents was determined as 80 minutes due to the disappearance of DMC and EMC gas emissions and considering the energy efficiency of the process.

The slight change in relative absorption intensity after 60 and 80 minutes, respectively, was attributed to the time it takes to entirely flush the gas cell. It is important to point out that the relative absorption intensity levels are slightly above 0. Traces of condensed electrolyte solvents on the gas cell walls and inside the exhaust gas pipe were assumed to be the main reason.

Besides the characteristic peaks of the electrolyte solvents (DMC, EMC, and EC), additional peaks between 4000 cm^{-1} and 3600 cm^{-1}, 1428 cm^{-1}, 1416 cm^{-1}, 1404 cm^{-1}, and 991 cm^{-1} were observed in the In-Situ FT-IR spectra of the thermal treatment exhaust gas in all experimental sets. Fig. 11 shows In-Situ FT-IR spectra of the exhaust gas of the thermal treatment process at 130 °C at various times. The peaks were identified as the characteristic peaks of HF (4000 cm^{-1}–3600 cm^{-1}) and POF_3 (1428 cm^{-1}, 1416 cm^{-1}, 1404 cm^{-1} and 991 cm^{-1}) [10,13,28].

The highly toxic gases HF and POF_3 are the decomposition products of the conductive salt $LiPF_6$ in contact with moisture/water. Anhydrous $LiPF_6$ generally decomposes thermally in a dry and inert environment to form solid LiF and gaseous PF_5 (Eq. (2)). In a humid

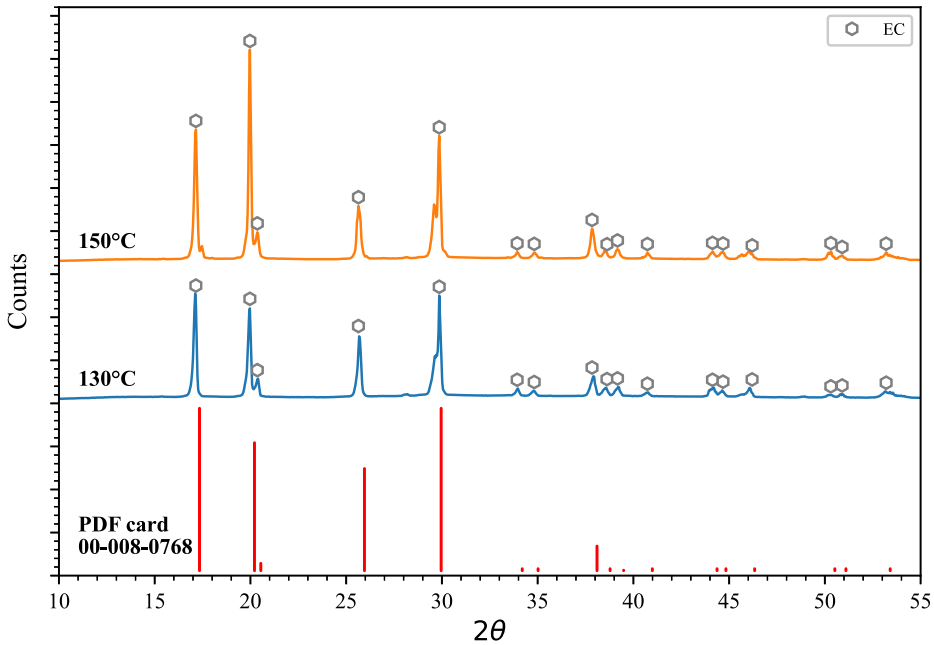

Fig. 8. XRD pattern of the recovered condensate after thermal treatment at 130 °C and 150 °C in the range from 10° to 55° 2Θ.

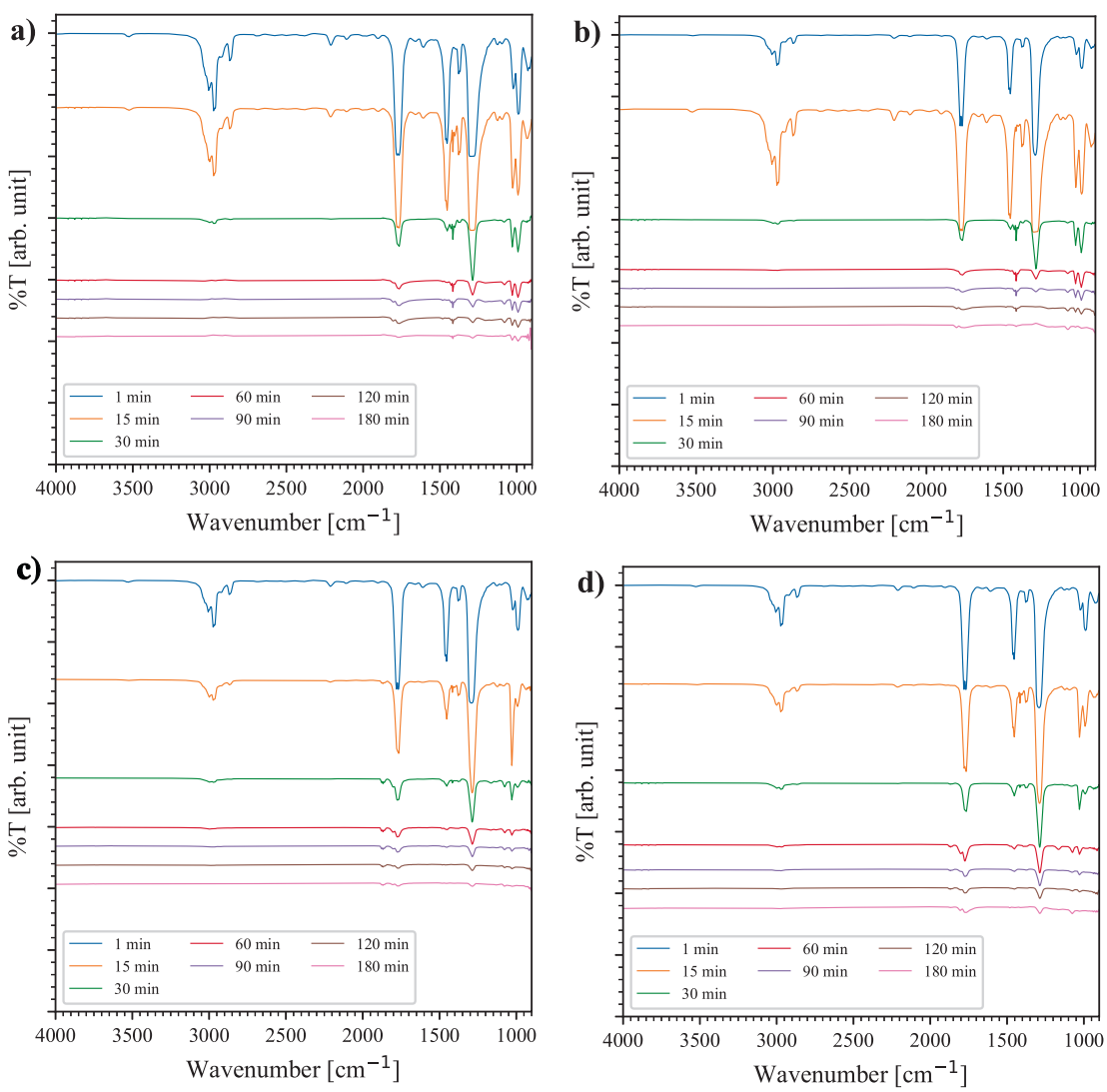

Fig. 9. In-Situ FT-IR spectra of the thermal treatment process exhaust gas after 1, 15, 30, 60, 90, 120, and 180 min at (a) 90 °C, (b) 110 °C, (c) 130 °C, and (d) 150 °C.

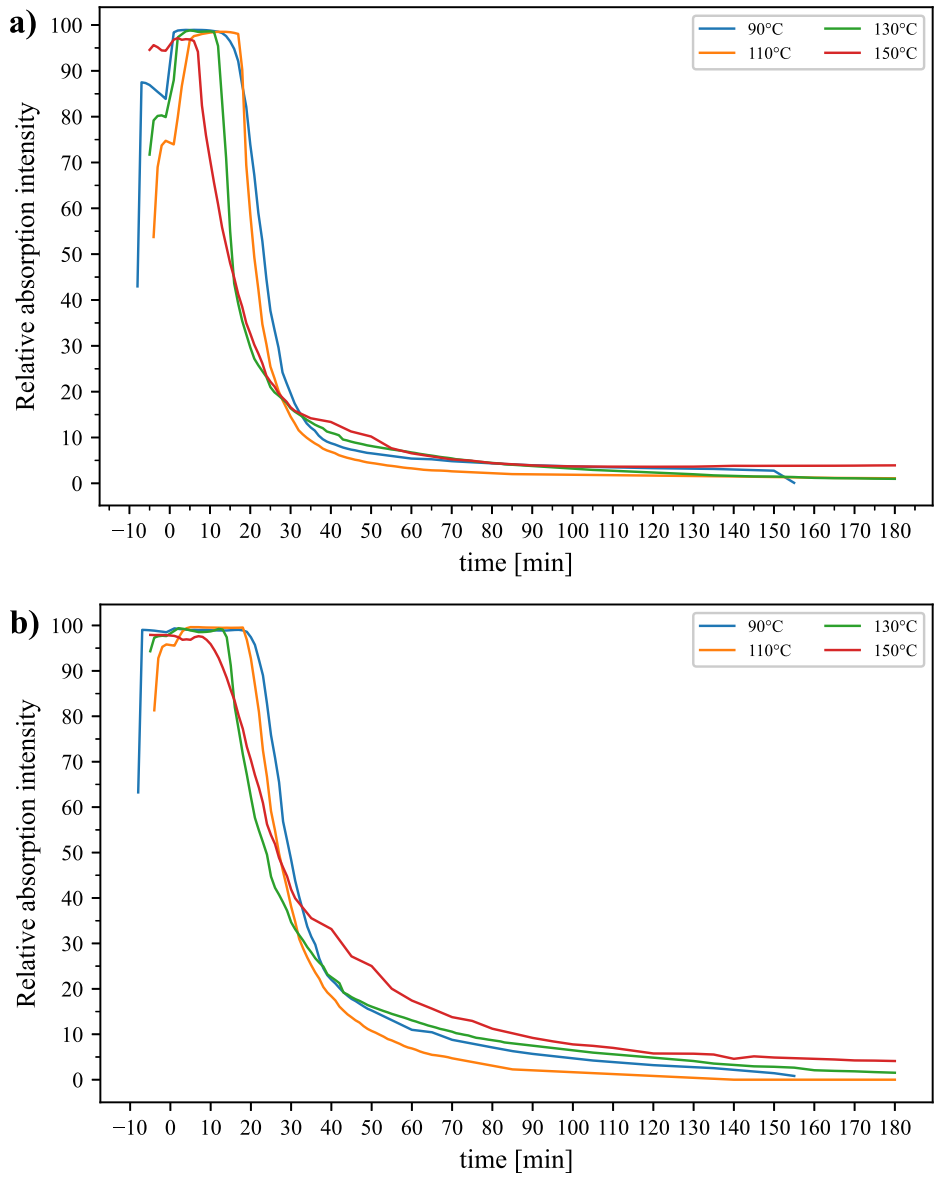

Fig. 10. Relative absorption intensity over the thermal treatment process time of 180 minutes of the (a) C=O peak of DMC at 1780 cm^{-1} and (b) O-C-O peak of EMC at 1284 cm^{-1}.

environment, PF_5 may further hydrolyze to form POF_3 and HF (Eq. (3)). However, even at trace amount of moisture/water, $LiPF_6$ may directly endothermically decompose to form solid LiF, and gaseous POF_3, and HF (Eq. (4)) [13,21,28–31].

$$LiPF_6 \rightarrow LiF(s) + PF_5(g) \tag{2}$$

$$PF_5(g) + H_2O(g) \rightarrow POF_3(g) + 2HF(g) \tag{3}$$

$$LiPF_6 + H_2O \rightarrow LiF(s) + POF_3(g) + 2HF(g) \tag{4}$$

The thermal stability of $LiPF_6$ is poor, and its onset decomposition temperature is still highly debated in the literature. According to Kock et al. [21], the onset point for anhydrous $LiPF_6$ is at 134.84 °C, while the hydrolysis reaction starts at 114.46 °C. However, in the presence of carbonate solvents, EC, EMC, and DMC, and moisture, gaseous POF_3 and HF were observed below 90 °C in the literature [10,28,29]. The hydrolysis degradation step is very sensitive to the water concentration and was observed at 300 ppm H_2O at 87 °C in the literature [28]. It is assumed that the moisture/humidity responsible for the hydrolysis decomposition (Eq. (4)) of the conductive salt ($LiPF_6$) was absorbed into the sample during the cell disassembly, the sample preparation process, and the subsequent storage of the cell at −18 °C, where the water vapor froze on the sample surface.

The characteristic peaks of the gaseous anhydrous decomposition product PF_5 at 1018 cm^{-1} and 946 cm^{-1} overlap with the vibrational peaks of the organic solvents [28]. Therefore, traces of PF_5 were challenging to identify with high certainty, but their occurrence should not be ruled out. In the literature, carbon dioxide (CO_2), carbon monoxide (CO), ethene (C_2H_4) and, dimethyl ether (C_2H_6O) are degradation products of DMC, EMC, and EC at temperatures above 180 °C [32]. However, in this low temperature thermal treatment approach no characteristic CO_2, CO, C_2H_4, and C_2H_6O peaks were detected in the exhaust gas at the process temperatures of 90 °C, 110 °C, 130 °C, and 150 °C. This is proof that the electrolyte solvents (DMC, EMC, and EC) were successfully recovered by the low temperature thermal treatment process.

It is crucial to detect the release period of the detected toxic gases (HF and POF_3) during the suggested process to design a proper exhaust gas treatment system. The time dependent changes

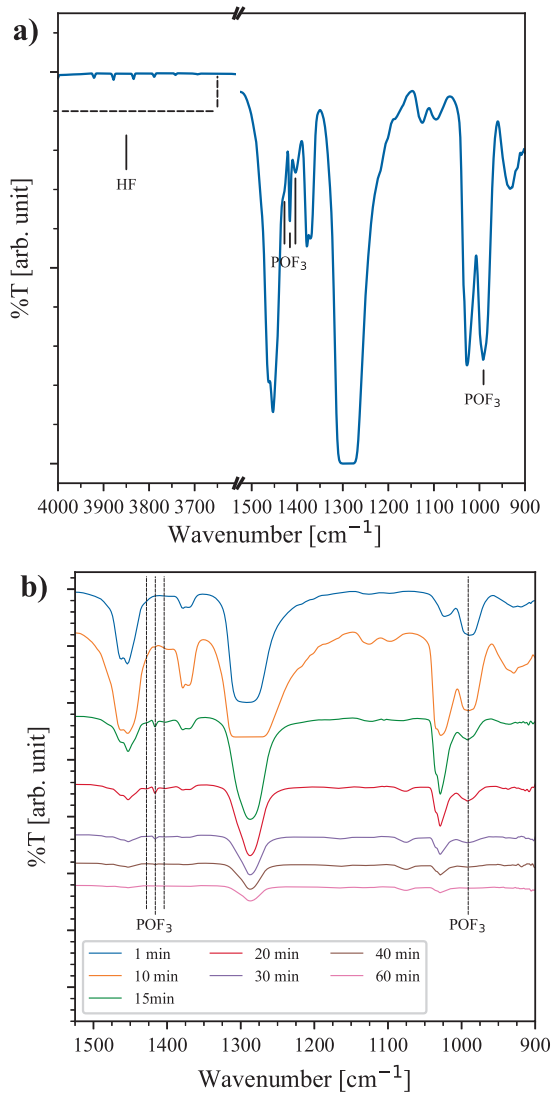

Fig. 11. FT-IR spectra of the exhaust gas measured at various times after the start of the thermal treatment process at 130 °C. (a) 13 min and (b) 1, 10, 15, 20, 30, 40, and 60 min.

of the vibrational peak intensities of HF and POF_3 in the In-Situ FITR exhaust gas spectra were studied to analyze the hydrolysis degradation reaction dependency on the process temperature and release period. The relative absorption intensity of the strong characteristic peaks at 3878 cm^{-1} (HF) and 1416 cm^{-1} (POF_3) were plotted over the process time of 180 minutes, as given in Figure S3.

Simultaneous emission of HF and POF_3 appeared at 4 to 10 minutes of the process. This confirms the hydrolysis degradation reaction of the conductive salt during the thermal treatment process. A correlation between the degradation time span and the process temperature was observed. A higher process temperature causes a shorter degradation time span. Whereas the relative absorption intensity diverges to a constant level after maximum 70 minutes for 130 °C and 150 °C, respectively, the POF_3 peak did not converge to zero value for 90 °C and 110 °C over the entire process time. Therefore, it can be concluded that $LiPF_6$ did not entirely degrade within the process time of 180 min at 90 °C and 110 °C but was fully decomposed at 130 °C and 150 °C. This is in alignment with recent studies where a weight percentage drop of $LiPF_6$ to 17 wt %, the proportion of LiF, at temperatures up to 150 °C was observed in a TG analysis [27].

The exhaust gas was passed through gas washing bottles to trap the HF and POF_3. The gaseous HF reacts with water to form hydrofluoric acid and in contact with water POF_3 forms phosphoric acid and HF following the hydrolysis steps (eq. (5)–(7)):

$$POF_3 + H_2O \rightarrow HPO_2F_2 + HF \quad (5)$$

$$HPO_2F_2 + H_2O \rightarrow H_2PO_3F + HF \quad (6)$$

$$H_2PO_3F + H_2O \rightarrow H_3PO_4 + HF \quad (7)$$

Analysis of the gas washing water resulted in a pH value of 1.9. The presence of HF and H_3PO_4 in the gas washing water was analyzed by IC. The corresponding chromatograph plotted in Figure S4 shows distinctive peaks at retention times for 2.8 min and 10.8 min, which were identified as F^- and PO_4^{3-}. Accordingly, HF and POF_3 were removed from the exhaust gas stream and simultaneously recovered as hydrofluoric acid and phosphoric acid. Although HF and POF_3 are hazardous, their reaction products, hydrofluoric acid and H_3PO_4, can be considered as a by-product of the process and potentially reutilized.

Conclusion

A low temperature thermal treatment process at four different process temperatures (90 °C, 110 °C, 130 °C, 150 °C) for the recovery of the electrolyte of spent EV LiBs was investigated. The linear and cyclic carbonates DMC, EMC and EC used as the organic solvent in the electrolyte were successfully recovered in liquid phase by the suggested low temperature thermal treatment. Results showed that the majority of EC was recovered in the pure solid phase. The optimum process parameters for the recovery of the maximum amount of electrolyte solvent were determined to be 80 min at 130 °C process temperature. Between 10 and 70 min of the process, gaseous HF and POF_3 were detected in the exhaust gas. By bubbling the process gas through gas washing bottles filled with MQ water, the highly toxic and corrosive HF and POF_3 were effectively recovered before releasing into the environment. Thereby, hydrofluoric acid and phosphoric acid were produced as a process by-product. The results showed that low temperature thermal treatment is a promising approach to recover the electrolyte from Li-ion battery waste prior to the metal recycling stage. However, further research is needed to improve the collection efficiency of the electrolyte solvents and to study the reuse of the recovered electrolyte solvent.

Declaration of Competing Interest

The authors declare the following financial interests/personal relationships which may be considered as potential competing interests: Burcak Ebin reports financial support was provided by Swedish Energy Agency.

Acknowledgements

Funding: This work was supported by the Swedish Energy Agency Battery Fund Program [Project No:50124-1].

Appendix A. Supplementary material

Supplementary data to this article can be found online at https://doi.org/10.1016/j.jiec.2022.11.020.

References

[1] N. Nitta, F. Wu, J.T. Lee, G. Yushin, Mater. Today 252–264. 10.1016/j.mattod.2014.10.040.

[2] J.M. Tarascon, M. Armand, Nature (2001) 359–367, https://doi.org/10.1038/35104644.
[3] E. Mossali, N. Picone, L. Gentilini, O. Rodrìguez, J.M. Pérez, M. Colledani, J. Environ. Manage. 264 (2020), https://doi.org/10.1016/j.jenvman.2020.110500.
[4] European Commission, EUR-Lex - 02006L0066-20180704 - EN - EUR-Lex. Available at: https://eur-lex.europa.eu/legal-content/EN/TXT/?uri=CELEX%3A02006L0066-20180704. Accessed November 1, 2021.
[5] European Commission, EUR-Lex - 52020PC0798 - EN - EUR-Lex. Available at: https://eur-lex.europa.eu/legal-content/EN/TXT/?uri=CELEX:52020PC0798. Accessed November 1, 2021.
[6] ERPS, Proposal for a Regulation of the European Parliament and the Council concerning batteries and waste batteries, repealing Directive 2006/66/EC and amending Regulation (EU) No 2019/1020 Committee, n.d.
[7] F. Arshad, L. Li, K. Amin, E. Fan, N. Manurkar, A. Ahmad, J. Yang, F. Wu, R. Chen, ACS Sustain. Chem. Eng. 8 (2020) 13527–13554, https://doi.org/10.1021/acssuschemeng.0c04940.
[8] X. Zhong, W. Liu, J. Han, F. Jiao, W. Qin, T. Liu, C. Zhao, Waste Manag. 89 (2019) 83–93, https://doi.org/10.1016/j.wasman.2019.03.068.
[9] G. Zhang, X. Yuan, Y. He, H. Wang, W. Xie, T. Zhang, Waste Manag. 115 (2020) 113–120, https://doi.org/10.1016/j.wasman.2020.05.030.
[10] S. Bertilsson, F. Larsson, M. Furlani, I. Albinsson, B.E. Mellander, J. Power Sources 365 (2017) 446–455, https://doi.org/10.1016/j.jpowsour.2017.08.082.
[11] F. Diaz, Y. Wang, R. Weyhe, B. Friedrich, Waste Manag. 84 (2019) 102–111, https://doi.org/10.1016/j.wasman.2018.11.029.
[12] K. Xu, Chem. Rev. 104 (10) (2004) 4303–4417, https://doi.org/10.1021/cr030203g.
[13] P. Andersson, P. Blomqvist, A. Lorén, F. Larsson, Fire Mater. 40 (8) (2016) 999–1015, https://doi.org/10.1002/fam.2359.
[14] N.P. Lebedeva, L. Boon-Brett, J. Electrochem. Soc. 163 (6) (2016) A821–A830, https://doi.org/10.1149/2.0171606jes.
[15] S. Nowak, M. Winter, Molecules 22 (2017) 3, https://doi.org/10.3390/molecules22030403.
[16] J. Marshall, D. Gastol, R. Sommerville, B. Middleton, V. Goodship, E. Kendrick, Metals (Basel). 10 (6) (2020) 773, https://doi.org/10.3390/met10060773.
[17] M. Grützke, V. Kraft, W. Weber, C. Wendt, A. Friesen, S. Klamor, M. Winter, S. Nowak, J. Supercrit. Fluids 94 (2014) 216–222, https://doi.org/10.1016/j.supflu.2014.07.014.
[18] M. Grützke, X. Mönnighoff, F. Horsthemke, V. Kraft, M. Winter, S. Nowak, RSC Adv. 5 (54) (2015) 43209–43217, https://doi.org/10.1039/c5ra04451k.
[19] D. Mu, Y. Liu, R. Li, Q. Ma, C. Dai, New J. Chem. 41 (15) (2017) 7177–7185, https://doi.org/10.1039/c7nj00771j.
[20] K. He, Z.Y. Zhang, L. Alai, F.S. Zhang, J. Hazard. Mater. 375 (2019) 43–51, https://doi.org/10.1016/j.jhazmat.2019.03.120.
[21] L.D. Kock, M.D.S. Lekgoathi, P.L. Crouse, B.M. Vilakazi, J. Mol. Struct. 1026 (2012) 145–149, https://doi.org/10.1016/j.molstruc.2012.05.053.
[22] NIST Standard Reference Data Program, Carbonic acid, dimethyl ester; Infrared Spectrum. Available at: https://webbook.nist.gov/cgi/cbook.cgi?ID=C616386&Type=IR-SPEC&Index=0#IR-SPEC. Accessed August 6, 2021.
[23] H. Bohets, B.J. Van Der Veken, Phys. Chem. Chem. Phys. 1 (8) (1999) 1817–1826, https://doi.org/10.1039/a901046g.
[24] A.K. Das, K. Sunanda, B.N. Rajasekhar, J. Quant. Spectrosc. Radiat. Transf. 272 (2021), https://doi.org/10.1016/j.jqsrt.2021.107789.
[25] B. Fortunato, P. Mirone, G. Fini, Spectrochim. Acta Part A Mol. Spectrosc. 27 (9) (1971) 1917–1927, https://doi.org/10.1016/0584-8539(71)80245-3.
[26] B.P. Kar, N. Ramanathan, K. Sundararajan, K.S. Viswanathan, J. Mol. Struct. 1072 (1) (2014) 61–68, https://doi.org/10.1016/j.molstruc.2014.04.044.
[27] S.E. Sloop, J.K. Pugh, S. Wang, J.B. Kerr, K. Kinoshita, Electrochem. Solid-State Lett. 4 (2001) 4, https://doi.org/10.1149/1.1353158.
[28] H. Yang, G.V. Zhuang, P.N. Ross, J. Power Sources 161 (1) (2006) 573–579, https://doi.org/10.1016/j.jpowsour.2006.03.058.
[29] B. Ravdel, K.M. Abraham, R. Gitzendanner, J. DiCarlo, B. Lucht, C. Campion, J. Power Sources Elsevier 119–121 (2003) 805–810.
[30] X.G. Teng, F.Q. Li, P.H. Ma, Q. Du Ren, S.Y. Li, Thermochim. Acta 436 (1–2) (2005) 30–34, https://doi.org/10.1016/j.tca.2005.07.004.
[31] S.F. Lux, I.T. Lucas, E. Pollak, S. Passerini, M. Winter, R. Kostecki, Electrochem. Commun. 14 (1) (2012) 47–50, https://doi.org/10.1016/j.elecom.2011.10.026.
[32] Z. Liao, S. Zhang, Y. Zhao, Z. Qiu, K. Li, D. Han, G. Zhang, T.G. Habetler, J. Energy Chem. 49 (2020) 124–135, https://doi.org/10.1016/j.jechem.2020.01.030.